THE JOURNAL OF PHYSICAL CHEMISTRY C

ARTICLE

pubs.acs.org/JPCC

Parallelly and Normally Surface-Aligned Organic Nanofiber Arrays

Kirill Bordo,[†] Manuela Schiek,*[,†] Aghiad Ghazal,[†] Ivonne Wallmann,[‡] Arne Lützen,[‡] Frank Balzer,[†] and Horst-Günter Rubahn[†]

[†]University of Southern Denmark, Mads Clausen Institute, NanoSYD, Alsion 2, DK-6400 Sønderborg, Denmark

[‡]Rheinische Friedrich-Whilhelms-University of Bonn, Kekulé-Institute of Organic Chemistry and Biochemistry, Gerhard-Domagk-Strasse 1, D-53121 Bonn, Germany

ABSTRACT: Results are presented from a direct comparison of 2,7-diphenylcarbazole (DPC) nanofibers fabricated in the form of parallel to the surface plane aligned arrays by means of organic molecular beam deposition (OMBD) and fabricated in the form of normal to the surface aligned arrays by solution-assisted wetting of porous anodic alumina (PAA) membranes. The former method leads to the formation of mutually aligned needlelike nanoaggregates on muscovite mica substrates, while the latter method allows fabrication of arrays of closely packed upright standing nanofibers. The dimensions of the DPC nanofibers obtained by the OMBD technique depend strongly on the nominal film thickness and on the substrate temperature during deposition. The DPC nanofibers obtained by template wetting possess the same shape and dimensions as those of the pores of the PAA template. All of the obtained nanofibers show strong polarization anisotropy, but the polarization dependent measurements indicate a higher degree of mutual alignment of the DPC molecules in the fibers obtained by OMBD as compared to those obtained by membrane wetting. Temperature dependent fluorescence spectra from the DPC nanoaggregates reveal blue shifts and narrowing of the spectral peaks with decreasing temperature as well as a redistribution of peak intensities.

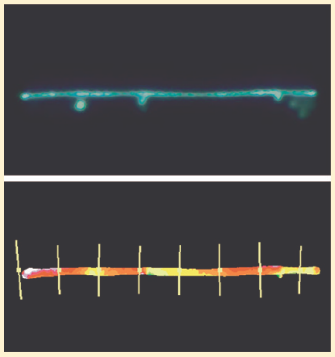

INTRODUCTION

Aggregates from π-conjugated organic molecules (such as, e.g., oligothiophenes, perylenes, pentacenes, and oligo-*p*-phenylenes) are known to possess peculiar optical, electrical, and optoelectronical properties, namely, polarized emission of light following electrical or optical excitation. They have already successfully been used as active layers in field effect transistors, light-emitting diodes, full color displays, waveguides, and lasers.[1−6] These molecules are thermally stable and can be vapor deposited under high-vacuum conditions to give epitaxial thin films of high quality or oriented nanostructures. For the latter case, mutual alignment and orientation of the aggregates influence a possible device performance. Therefore, it is important to synthesize well-aligned nanowires or "nanofiber" arrays in a controllable manner.

Ideally, depending on the actual device to be developed, the nanofibers should either be oriented parallel or normal to the surface plane. For that purpose, two complementary methods are available, namely, organic molecular beam deposition (OMBD) and template wetting. OMBD has been successfully used to fabricate mutually horizontally aligned nanofibers on mica substrates.[7,8] In such cases, the anisotropy of the muscovite surface is believed to be responsible for the self-assembly of the deposited molecules along specific directions.[9−11] In particular, nanofibers from α-thiophenes, *p*-phenylenes, and thiophene/phenylene co-oligomers were generated by this approach.[12−17] A technique which allows fabrication of aligned 1D nanostructures normal to the surface is template wetting.[18] In this method, a porous template is filled by a solution or a melt. After selective removal of the template, arrays of nanofibers or nanotubes are obtained. In most cases, porous anodic alumina (PAA) templates are used. Such templates can have different pore diameters and interpore distances, depending on the fabrication conditions.[19,20] By using solution- and melt-assisted template wetting, nanotubes from, e.g., perylene[21] and pentacene[22] were obtained.

Here, we report on the fabrication of nanofibers from 2,7-diphenylcarbazole (DPC). Compounds containing a carbazole moiety processed to thin films were used in OLEDs,[23,24] displays,[25,26] and photovoltaic devices.[27−29] The fabrication of fluorescent nanotube arrays from unsubstituted carbazole by means of a template-assisted physical vapor deposition method has also been reported.[30] The structure of the DPC molecule is shown in Figure 1a. The nanofibers are obtained by means of OMBD on muscovite mica as well as by template wetting of commercially available PAA membranes.

Note that it is rather unusual that such an organic semiconductor molecule allows fabrication of nanostructures using both methods, vapor deposition and solution-assisted wetting. Many rodlike semiconductors molecules, which grow to nanofibers on a mica surface, are poorly soluble in all common solvents,[32] which renders solution-assisted wetting impossible. Here, for the first time a direct comparison of nanoaggregates obtained by the two growth methods using the same, optoelectronically interesting molecular building block is presented.

EXPERIMENTAL SECTION

The DPC used in the present work was synthesized according to a previously published protocol.[31] Briefly, Boc-protected

Received: May 28, 2011
Revised: September 5, 2011
Published: September 21, 2011

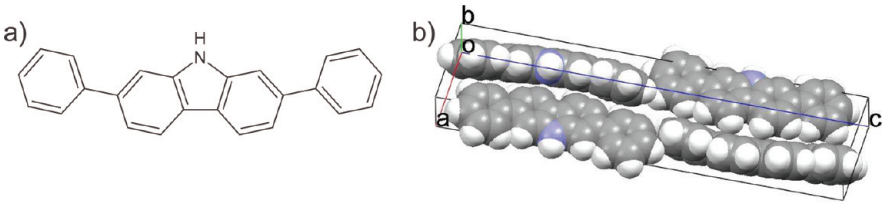

Figure 1. (a) Structural formula of DPC and (b) crystal structure of bulk DPC obtained from X-ray diffraction data.[31]

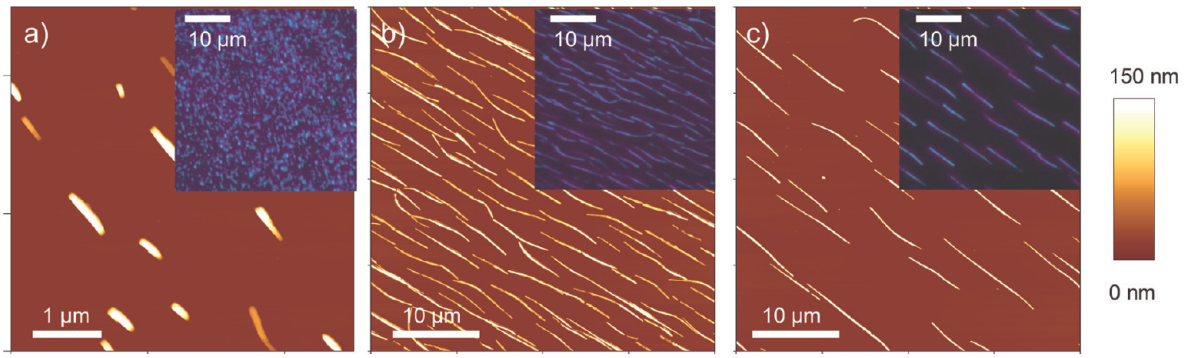

Figure 2. AFM images and fluorescence microscopy images (insets, excitation wavelength λ_{exc} = 365 nm) of DPC nanoaggregates on muscovite mica. Surface temperatures T_{sub} during deposition: 300 (a), 330 (b), and 370 K (c). The nominal film thickness for all images is 4 nm.

2,7-dibromcarbazole was subjected to a twofold Suzuki cross-coupling with phenylboronic acid, deprotected in situ and recrystallized to give the DPC in a yield of 73%.

By using the OMBD technique, DPC nanofibers are grown on mica under high-vacuum conditions. Muscovite mica sheets (grade V-4, Structure Probe, Inc.) are cleaved in air and are transferred immediately into a vacuum chamber with a base pressure below 1×10^{-8} mbar. The deposition is performed from an oven at a vacuum pressure of the order of 2×10^{-7} mbar . The substrate temperature during deposition, T_{sub}, is varied from room temperature up to 390 K. The flux of DPC molecules as well as the total amount of deposited material is monitored by a water-cooled microbalance (Inficon XTC/2), displaying a maximum deposition rate of 0.02 nm/s.

For the fabrication of nanofibers by means of template wetting, commercial membrane filters (Anodisc) with mean pore diameters of 200 nm and a thickness of 60 μm are employed. Two DMSO solutions of DPC having different concentrations, i.e., a saturated solution and a 0.02 M solution, are used. The DPC is introduced into the pores by means of the "drip-and-dry" method. This method involves placing the template on a 50 °C hot plate and slowly dripping the precursor solution onto it. After each drop is added, the solvent is allowed to evaporate. After a prescribed number of "drip-and-dry" cycles (typically 20), a piece of the membrane is attached to an adhesive carbon pad and excess material is removed from the top of the membrane using a scalpel. Supported DPC nanofibers are obtained by selective dissolution of the supported membrane in 2 M aqueous NaOH for 5 h. Another piece of the same membrane is left unsupported and freed from excess material on both sides. In that case, nanofibers are freed by dissolution of the membrane (2 M aqueous NaOH, 5 h), rinsed several times in deionized water, and collected by centrifugation.

Optical images of the nanofiber arrays are obtained by a fluorescence microscope equipped with a high-pressure Hg lamp (Nikon Eclipse TE 300). Polarization measurements are performed using the same microscope with a rotational stage (Thorlabs PRM1) mounted on its sample holder. Temperature dependent fluorescence spectra of the DPC samples between room temperature and 6 K are obtained in a He-cryostat with the pressure in the sample chamber being lower than 5×10^{-5} mbar. Fluorescence of the DPC samples is excited by a He−Cd laser (λ_{exc} = 325 nm), and the spectra are acquired using a spectrograph coupled to a cooled CCD camera. Scanning electron microscopy (SEM) images of DPC nanofibers attached to a carbon pad are acquired using a Hitachi S-4800 operating at beam voltages of 1−5 kV. Samples are coated with gold (2 nm) to facilitate SEM imaging. Atomic force microscopy (AFM) is performed with a JPK Nanowizard operating in intermittent contact mode (Budget Sensors TAP 300, 10 nm tip radius).

RESULTS AND DISCUSSION

For DPC nanofibers obtained by OMBD, fluorescence microscopy images reveal brightly blue fluorescent DPC nanoaggregates on mica. The fibers are grown at different surface temperatures, and typical images are shown in Figure 2. Near room temperature only small aggregates are formed on the substrate (Figure 2a). If the surface temperature during deposition is increased to 330 K, a few micrometer long fibers are formed (Figure 2b). These fibers are generally well aligned, but some of them show bends and kinks. An increase in surface temperature to 370 K results in longer fibers with fewer kinks (Figure 2c). Increasing the surface temperature further obstructs needle growth. With the help of a "Schlagfigur"[33,34] it has been found that the mean fiber direction is parallel to one of the muscovite [110] directions, very similar to the behavior of other *p*-phenylenes and 2,5-di-4-biphenylthiophene (PPTPP) grown on mica.[10,16]

Atomic force microscopy investigations give structural information about the nanofibers. Here, even for deposition at room temperature mutually aligned, needlelike aggregates are resolved.

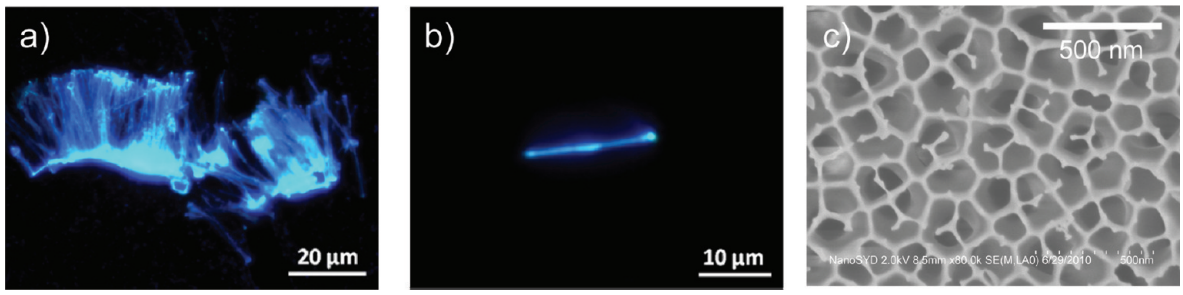

Figure 3. Fluorescence microscopy images of DPC nanofibers obtained by wetting of a PAA template: a bundle of nanofibers lying on a carbon pad (a) and a single nanofiber (or a bundle of few fibers) isolated via centrifugation (b). In (c) a top-view SEM image of a commercial PAA membrane (Anodisc) is presented.

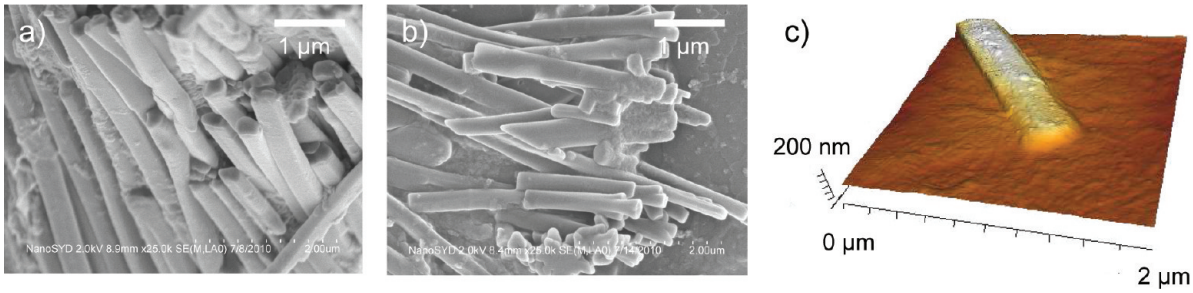

Figure 4. SEM images of DPC nanofibers obtained by wetting of a PAA template: by a saturated solution of DPC (a) and by a diluted (0.02 M) solution of DPC (b). In (c) a $2 \times 2\ \mu m^2$ AFM image of a single DPC nanofiber obtained by template wetting is shown.

The fibers are generally longer, higher, and wider for the elevated temperatures as expected from basic nucleation theory,[35] their lengths reaching almost 20 μm. For 4 nm nominal thickness, average heights increase from 100 to 190 nm with increasing deposition temperature. Fiber widths are of the order of 100−300 nm. Especially the longer fibers are built up of segments of different heights and often taper at the endings (not shown).

Fluorescence microscopy images of the DPC nanofibers obtained by wetting of a PAA template by a saturated DPC solution are presented in Figure 3. Figure 3a shows a bundle of blue-light emitting nanofibers, which stick to the surface of a carbon pad after complete dissolution of the porous template. The fibers are merged together on one side. Bright blue-light emitting regions on the image correspond probably to some excess of the DPC which did not diffuse into the pores of the template. In Figure 3b a single DPC nanofiber (or a bundle of a few fibers) isolated by centrifugation is displayed. The mean nanofiber length estimated from the fluorescence microscopy images is about 30 μm which is two times less than the pore depth of the PAA template (60 μm). This is because the employed number of "drip-and-dry" cycles was not high enough to fill all the pores of the template completely. Some of the fibers could also get broken during the template removal procedure. The major drawback of the solution-assisted wetting procedure is the difficulty in removing the template completely and cleaning the fibers from sodium hydroxide remnants. Residues from the template removal procedure can be seen in both SEM and AFM images, Figure 4.

In a top-view SEM image of a commercial PAA membrane (Anodisc) image, Figure 3c, individual pore openings are clearly seen. The pores have an irregular shape and are not well arranged, which is a characteristic of a single-step anodization process. The pore openings are funnel-shaped. Over the pore openings a very thin porous layer with lower pore diameters and interpore distances is present. Figure 4a shows a bundle of DPC nanofibers obtained after the wetting of a template by a saturated DPC solution. The nanofibers have the same diameters as those of the template pores (about 250 nm). Some of them are slightly bent due to their mechanical flexibility. The residue which is observed in between the fibers is probably either the alumina which was not dissolved completely during the template removal or the crystallized NaOH residue which was not completely removed by rinsing in water. In Figure 4b DPC nanofibers obtained by wetting of a template by a diluted (0.02 M) DPC solution are shown. The as-prepared nanofibers are quite short (less than 2 μm) if compared to those obtained with the use of a saturated DPC solution. Apparently, in the case of lower concentrations the lack of material inside the template pores does not allow the formation of longer structures. The tips of the fibers show a characteristic funnel-like shape originating from the initial surface morphology of the porous template.

Figure 4c shows an AFM scan of a single DPC fiber made by template wetting, lying on a glass substrate and being partly buried in template or sodium hydroxide residues. As in the SEM images it is obvious that the shape of the fiber is not perfectly cylindrical but exhibits facets. These facets are most probably caused by the shape of the pores of the PAA template.

Polarization measurements performed on the as-fabricated DPC nanofibers reveal their strong polarization anisotropy. The fibers are illuminated with unpolarized UV light from a Hg lamp (λ_{exc} = 365 nm), and the emitted fluorescence is observed through a linear polarizer. To reduce polarization artifacts from the setup, the sample is rotated in steps of $\Delta\varphi = 5°$ over 360°, whereas the transmission axis of the polarizer remains fixed. For each angle a fluorescence image is taken, resulting in a total number of $N = 72$ images. For the intensity variation of a series of pixels $I_n^{x,y}(n\Delta\phi)$ with $n = 0, 1, ..., N - 1$, the Fourier

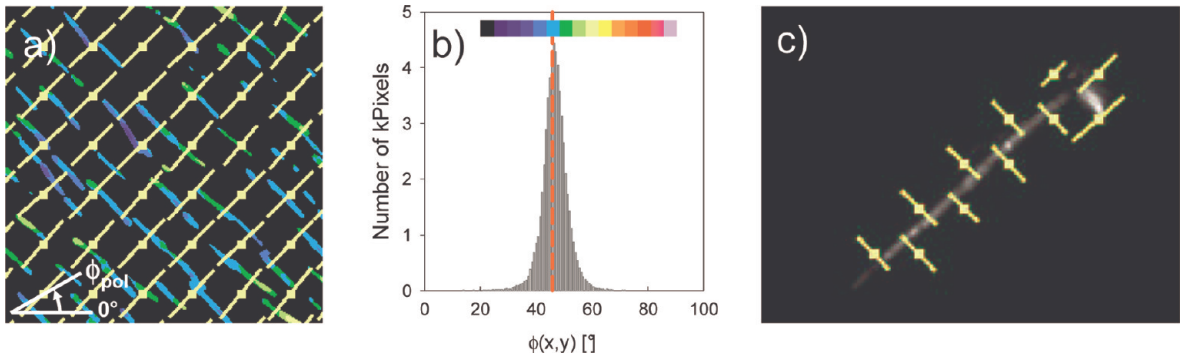

Figure 5. (a) Polarization angle ϕ_{pol} for the maximum in emitted fluorescence of a sample of OMBD grown DPC nanofibers (image size 40 × 40 μm^2); for the color coding, see (b). The yellow lines emphasize the mean local polarization direction. (b) Histogram of the polarization angles for a larger area, together with the angle perpendicular to the mean fiber orientation (vertical dashed red line). (c) Local polarization directions for two bundles of template-grown DPC fibers (a short and a long one); the length of the long fiber is 30 μm.

coefficients

$$\tilde{I}_\gamma(x,y) = \frac{1}{N}\sum_{n=0}^{N-1} I_n^{x,y}\, e^{-i2\pi\gamma n/N}$$

are calculated.[36] The discrete Fourier spectrum is dominated by the $\gamma = 0$ and $\gamma = 2$ coefficients. For the polarization dependent fluorescence the complex-valued second Fourier coefficient $\tilde{I}_{\gamma=2}(x,y)$ is determined, and from that the angle $\phi_{pol}(x,y)$, under which the emitted fluorescence for pixel (x, y) has its maximum value

$$\phi_{pol}(x,y) = \frac{1}{2}\arg \tilde{I}_{\gamma=2}(x,y)$$

In Figure 5a this angle $\phi_{pol}(x, y)$ is presented pixelwise for a DPC nanofiber sample. In Figure 5b the corresponding distribution of the angles together with the color code for Figure 5a is shown. The yellow lines in Figure 5a denote the average local polarization direction of the sample. Obviously, the mean polarization direction is perpendicular to the mean needle direction. Note that even for a single straight fiber the angle for maximum polarization often varies by a few degrees along the fiber, hinting to slightly different molecular orientations within the fiber. For bent fibers the polarization usually follows the bending. The structure of a DPC single crystal obtained from X-ray diffraction data is shown schematically in Figure 1b.[31] DPC crystallizes in a monoclinic unit cell with $Z = 4$ molecules per unit cell and lattice parameters $a = 7.5147(9)$ Å, $b = 6.7446(5)$ Å, $c = 36.382(4)$ Å, and $\beta = 95.684(10)°$. Within the unit cell the molecules adopt the herringbone packing mode. As long as there is no intermolecular photophysical interaction in the excited state, the angle $\phi_{pol}(x, y)$ therefore corresponds approximately to the projection of the long molecular axis onto the substrate surface of all molecules within the image pixel (x, y). For OMBD growth the value of $\phi_{pol}(x, y)$ being perpendicular to the direction of the nanofibers' local long axes is in agreement with the results obtained for, e.g., PPTPP nanofibers on mica and results from a combination of surface growth epitaxy and molecular packing effects.[10,11,16,37]

The spatially resolved polarization ratio is defined as

$$\rho(x,y) = \frac{I_{max}(x,y) - I_{min}(x,y)}{I_{max}(x,y) + I_{min}(x,y)}$$

of the maximum (I_{max}) and minimum (I_{min}) fluorescence intensities at pixel (x, y). Due to the experimental setup, this parameter is more prone to systematic errors than the polarization angle $\phi_{pol}(x, y)$. Therefore, instead of presenting the spatial distribution of $\rho(x, y)$, only average values of the obtained distributions of $\rho(x, y)$ are given for the two types of samples. Photobleaching has been corrected via a single exponential decay.[38] For OMBD growth this results in an average value of $\rho = 0.85 \pm 0.1$. These findings have to be compared to template-fabricated DPC nanofibers, Figure 5c. The local polarization direction is again perpendicular to the local fiber direction. Again, this result suggests that the molecule's long axes are aligned perpendicular to the long fiber axis. The template-fabricated ones in general have lower values of the polarization ratio with a larger width of the distributions, peaking at $\rho = 0.45 \pm 0.25$. The difference in these values can be explained by the higher degree of molecular alignment within the nanofibers made by OMBD.

Figure 6 shows temperature dependent fluorescence spectra for DPC nanofibers grown by OMBD at the substrate temperature $T_{sub} = 370$ K (a) and by template wetting (b). Since all UV illumination for the measurements was performed at pressures lower than 5×10^{-5} mbar, no changes in the fluorescence spectra due to oxygen-induced photobleaching are observed. The structure of the spectra is mostly similar for the two samples under investigation. At room temperature the spectra from both samples consist of a single vibrational progression, probably mainly originating from the C−C stretching mode.[39,40] The three most pronounced vibronic peaks are (arbitrarily) named as 0−0, 0−1, and 0−2, Figure 6b. A decrease of the temperature leads to a rise of the overall fluorescence intensity, to a redistribution of relative peak intensities, and to the appearance of additional peaks. For a quantitative analysis, all of the spectra are fit with a set of Gaussians. From the fitting procedure individual peak positions, line widths (FWHMs), and relative intensities are determined. The energetic spacing between adjacent peaks is between 150 and 180 meV, with line widths between 70 and 130 meV at room temperature for the 0−0 and 0−1 peaks. The FWHM of the 0−0 peak is always narrower than the one for the 0−1 peak. The peak widths decrease monotonically with decreasing temperature, reaching values between 50 and 80 meV at a temperature of 6 K.

The 0−0 and 0−1 peaks (at room temperature at 3.19 and 3.05 eV, respectively) show a blue shift with decreasing temperature. Depending on the fabrication method, the shift is between 15 and 50 meV. The blue shift in low-temperature fluorescence spectra was also observed for *p*-6P nanofibers.[41,42] It was

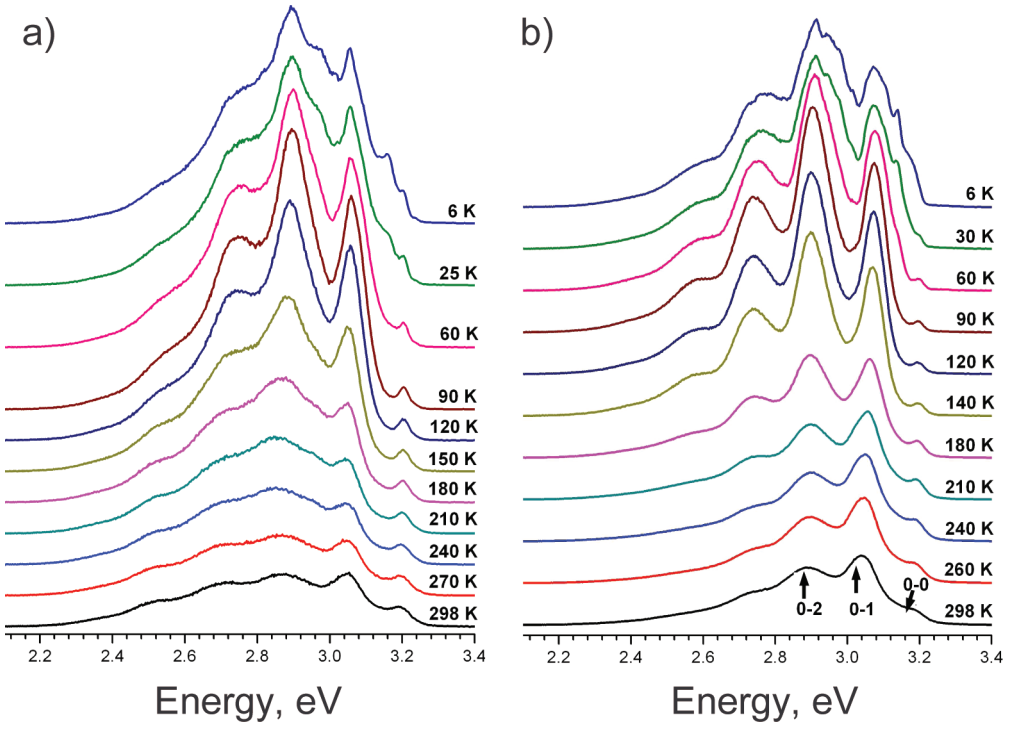

Figure 6. Temperature dependent fluorescence spectra for DPC nanofibers obtained by OMBD (growth temperature T_{sub} = 370 K) (a) and by template wetting (b).

attributed to exciton−phonon interactions, the probability of which decreases with decreasing temperature. For temperatures below 90 K, the fluorescence spectra cannot be fitted with the same set of peaks which is used for higher temperatures. Additional peaks have to be introduced between 0−0 and 0−1 peaks and also between 0−1 and 0−2 peaks. These additional peaks show the same behavior as the 0−0 and 0−1 peaks; namely, they shift to the blue with decreasing temperature, and their line widths also decrease. Furthermore, the relative intensities of these peaks increase when decreasing the temperature from 90 to 6 K. The appearance of additional peaks in the high-energy part of a fluorescence spectrum was reported for *p*-6P nanofibers.[41,42] The nature of these peaks is so far unresolved.

CONCLUSION

In summary, DPC nanofibers have been manufactured by means of two techniques: organic molecular beam deposition and solution-assisted template wetting. By the OMBD technique, well-aligned blue-light emitting nanoaggregates on muscovite mica are obtained. The aggregates are oriented along one of the high-symmetry [110] directions on the muscovite mica (001) face, suggesting a similar nanofiber formation process as observed for, e.g., the *p*-phenylenes. The dimensions of the nanofibers depend on the deposition temperature and on the nominal film thickness. As predicted from nucleation theory, an increase in substrate temperature during deposition leads to a lower number density of larger aggregates. By the template wetting technique, arrays of closely packed nanofibers are obtained. Here, the diameters of the nanofibers are the same as those of the template pores, and the length of the nanofibers depends on the concentration of the wetting solution, being higher for the saturated solution. The obtained nanofibers show strong polarization anisotropy. The polarization ratio was found to be around $\rho = 0.85 \pm 0.1$ for nanofibers obtained by OMBD and around $\rho = 0.45 \pm 0.25$ for nanofibers obtained by template wetting. This indicates a higher degree of mutual alignment of DPC molecules in the fibers obtained by vapor growth due to the interplay of intermolecular and aligning molecule−surface forces. In the case of template wetting, the molecule−surface forces are less well directed, eventually leading to a less perfect crystalline growth. Detailed analysis of the temperature dependent fluorescence spectra from the as-prepared DPC nanoaggregates reveals many of the trends reported for *p*-6P nanofibers,[37] namely, blue shifts and narrowing of the spectral peaks with decreasing temperature and redistribution of peak intensities.

The ability to synthesize 1D nanostructures based on π-conjugated organic molecules such as diphenylcarbazole in arrays that are oriented parallel or normal to the surface is an important step forward toward the realization of new organic nanowire and nanotube optoelectronic devices with tailored functionalities.

AUTHOR INFORMATION

Corresponding Author

*E-mail: schiek@mci.sdu.dk.

ACKNOWLEDGMENT

The authors are grateful to the Danish research agencies FNU and FTP as well as the Danish Advanced Technologies Trust for supporting this work by various grants. A.L. thanks the German research foundation DFG for financial support.

REFERENCES

(1) Forrest, S. *Nature* **2004**, *428*, 911–918.
(2) Schenning, A.; Meijer, E. *Chem. Commun.* **2005**, 3245–3258.

(3) Cicoira, F.; Santato, C. *Adv. Funct. Mater.* **2007**, *17*, 3421–3434.
(4) Tessler, N. *Adv. Mater.* **1999**, *11*, 363–370.
(5) Quochi, F.; Cordella, F.; Mura, A.; Bongiovanni, G.; Balzer, F.; Rubahn, H.-G. *J. Phys. Chem. B* **2005**, *109*, 21690–21693.
(6) Balzer, F.; Bordo, V.; Simonsen, A.; Rubahn, H.-G. *Phys. Rev. B* **2003**, *67*, 115408.
(7) Andreev, A.; Matt, G.; Brabec, C.; Sitter, H.; Badt, D.; Seyringer, H.; Sariciftci, N. *Adv. Mater.* **2000**, *12*, 629–633.
(8) Balzer, F.; Rubahn, H.-G. *Appl. Phys. Lett.* **2001**, *79*, 3860–3862.
(9) Kuwahara, Y. *Phys. Chem. Miner* **2001**, *28*, 1–8.
(10) Balzer, F.; Schiek, M.; Al-Shamery, K.; Lützen, A.; Rubahn, H.-G. *J. Vac. Sci. Technol., B* **2008**, *26*, 1619–1623.
(11) Simbrunner, C.; Nabok, D.; Hernandez-Sosa, G.; Oehzelt, M.; Djuric, T.; Resel, R.; Romaner, L.; Puschnig, P.; Ambrosch-Draxl, C.; Salzmann, I.; Schwabegger, G.; Watzinger, I.; Sitter, H. *J. Am. Chem. Soc.* **2011**, *133*, 3056–3062.
(12) Schiek, M.; Lützen, A.; Al-Shamery, K.; Balzer, F.; Rubahn, H.-G. *Cryst. Growth Des.* **2007**, *7*, 229–233.
(13) Kankate, L.; Balzer, F.; Niehus, H.; Rubahn, H.-G. *Thin Solid Films* **2009**, *518*, 130–137.
(14) Balzer, F.; Rubahn, H.-G. *Surf. Sci.* **2004**, *548*, 170–182.
(15) Teichert, C.; Hlawacek, G.; Andreev, A.; Sitter, H.; Frank, P.; Winkler, A.; Sariciftci, N. *Appl. Phys. A: Mater. Sci. Process.* **2006**, *82*, 665–669.
(16) Balzer, F.; Schiek, M.; Lützen, A.; Rubahn, H.-G. *Chem. Mater.* **2009**, *21*, 4759–4767.
(17) Schiek, M.; Balzer, F.; Al-Shamery, K.; Lützen, A.; Rubahn, H.-G. *J. Phys. Chem. C* **2009**, *113*, 9601–9608.
(18) Thomas, A.; Goettmann, F.; Antonietti, M. *Chem. Mater.* **2008**, *20*, 738–755.
(19) Steinhart, M.; Wehrspohn, R.; Gösele, U.; Wendorff, J. *Angew. Chem., Int. Ed.* **2004**, *43*, 1334–1344.
(20) Lee, W.; Ji, R.; Gösele, U.; Nielsch, K. *Nat. Mater.* **2006**, *5*, 741–747.
(21) Zhao, L.; Yang, W.; Ma, Y.; Yao, J.; Li, Y.; Liu, H. *Chem. Commun.* **2003**, 2442–2443.
(22) Barrett, C.; Iacopino, D.; O'Carroll, D.; De Marzi, G.; Tanner, D.; Quinn, A.; Redmond, G. *Chem. Mater.* **2007**, *19*, 338–340.
(23) Lee, J.-H.; Woo, H.-S.; Kim, T.-W.; Park, J.-W. *Opt. Mater.* **2002**, *21*, 225–229.
(24) Fischer, A.; Chenais, S.; Forget, S.; Castex, M.-C.; Ades, D.; Siove, A.; Denis, C.; Maisse, P.; Geffroy, B. *J. Phys. D: Appl. Phys.* **2006**, *39*, 917–922.
(25) Iwakuma, T.; Yamamoto, H.; Hironaka, Y.; Ikeda, H.; Hosokawa, C.; Tomita, S.; Arakane, T. Material for organic electroluminescence devices and organic electroluminescence device using the material. U.S. Patent 2004/0086745 A1.
(26) Sasaki, M.; Torii, M.; Sagisaka, T.; Okada, T.; Kawamura, S.; Adachi, C.; Kawamura, Y.; Muneuchi, K. 3, 6-Diphenylcarbazole compound and organic electroluminescent device. U.S. Patent 2005/0084711 A1.
(27) Li, J.; Dierschke, F.; Wu, J.; Grimsdale, A.; Müllen, K. *J. Mater. Chem.* **2006**, *16*, 96–100.
(28) Boudreault, P.-L.; Blouin, N.; Leclerc, M. *Adv. Polym. Sci.* **2008**, *212*, 99–124.
(29) Li, J.; Grimsdale, A. *Chem. Soc. Rev.* **2010**, *39*, 2399–2410.
(30) Shen, X.-P.; Yin, G.; Gao, C.; Xu, Z. *Mater. Chem. Phys.* **2009**, *113*, 202–207.
(31) Wallmann, I.; Schnakenburg, G.; Lützen, A. *Synthesis* **2009**, 79–84.
(32) Schiek, M.; Balzer, F.; Al-Shamery, K.; Lützen, A.; Rubahn, H.-G. *Soft Matter* **2008**, *4*, 277–285.
(33) Tröger, W. *Optische Bestimmung der Gesteinsbildenden Minerale*, 4th ed.; E. Schweizerbart'sche Verlagsbuchhandlung: Stuttgart, Germany, 1971.
(34) Jerome, B.; Shen, Y. *Phys. Rev. E* **1993**, *48*, 4556–4574.
(35) Ohring, M. *Materials Science of Thin Films*, 2nd ed.; Academic Press: New York, 2001.
(36) Bernchou, U.; Brewer, J.; Midtiby, H.; Ipsen, J.; Bagatolli, L.; Simonsen, A. *J. Am. Chem. Soc.* **2009**, *131*, 14130–14131.
(37) Kankate, L.; Balzer, F.; Niehus, H.; Rubahn, H.-G. *J. Chem. Phys.* **2008**, *128*, 084709.
(38) DeMay, B.; Bai, X.; Howard, L.; Occhipinti, P.; Meseroll, R.; Spiliotis, E.; Oldenbourg, R.; Gladfelter, A. *J. Cell Biol.* **2011**, *193*, 1065–1081.
(39) Cordella, F.; Quochi, F.; Saba, M.; Andreev, A.; Sitter, H.; Sariciftci, N.; Mura, A.; Bongiovanni, G. *Adv. Mater.* **2007**, *19*, 2252–2256.
(40) Poolmee, P.; Ehara, M.; Nakatsuji, H. *Theor. Chem. Acc.* **2011**, doi: 10.1007/s00214-011-0949-1.
(41) Guha, S.; Rice, J.; Tau, Y.; Martin, C.; Chandrasekhar, M.; Chandrasekhar, H.; Guentner, R.; Scanduicci de Freitas, P.; Scherf, U. *Phys. Rev. B* **2003**, *67*, 125204.
(42) Balzer, F.; Pogantsch, A.; Rubahn, H.-G. *J. Lumin.* **2009**, *129*, 784–789.